AIAA SciTech Forum
6-10 January 2020, Orlando, FL
AIAA Scitech 2020 Forum

10.2514/6.2020-0878

Relative Dynamics Modeling and Three-Dimensional Formation Control for Leader-Follower UAVs in the Presence of Wind

Amer Al-Radaideh*, Robert Selje†, and Liang Sun‡
New Mexico State University, Las Cruces, New Mexico, 88003, USA

This paper presents a three-dimensional (3D) formation controller for two unmanned aerial vehicles (UAVs) in the presence of wind. The relative dynamics of the leader-follower UAV team is derived based on a local-level spherical coordinate frame using only the local information, i.e., the relative distance between the two UAVs, the azimuth and elevation angles from both the leader's and the follower's viewpoints, respectively. A formation controller is then derived using the Lyapunov-based backstepping technique that enables the tracking error of the leader-follower UAVs to exponentially converge to zero. The observability analysis was conducted and an extended Kalman filter was developed to estimate the wind difference between the leader and follower UAVs. The performance of the proposed formation control law is examined in simulation.

I. Nomenclature

r	=	line-of-sight vector from leader to follower, m
ρ	=	reciprocal of r, $1/m$
ℓ	=	subscript indicating leader
f	=	subscript indicating follower
V_a	=	UAV airspeed, represented by the velocity with respect to the surrounding air, m/s
V_g	=	ground speed, represented by the velocity with respect to the inertial frame, m/s
V_w	=	wind velocity relative to the inertial frame, m/s
γ	=	flight path angle, the angle between the horizontal plane and the ground velocity vector V_g, radian
γ_a	=	air-mass-referenced flight-path angle, the angle from the inertial North-East plane to V_a, radian
χ	=	course angel, radian
ψ	=	heading (yaw) angle, the angle between North and the UAV body x-axis, radian
η_f	=	follower azimuth angle, radian
η_l	=	leader azimuth angle, radian
ξ_l	=	elevation angle of the follower with respect to the leader in leader's vehicle-1 frame, radian
ξ_f	=	elevation angle of the leader with respect to the follower in follower's vehicle-1 frame, radian
w_l*	=	wind disturbance affecting the leadaer UAV in 3 directions $(*)$, north (n), east (e) and down (d), m/s
w_f*	=	wind disturbance affecting the follower UAV in 3 directions $(*)$, north (n), east (e) and down (d), m/s
V_*^c	=	air speed command, m/s
ϕ_*^c	=	roll angle command, radian
γ_{a*}^c	=	air-mass-referenced flight-path angle command, radian
R_*	=	rotation matrix
r^d	=	desired line-of-sight vector from leader to follower, m
η_f^d	=	desired follower azimuth angle, radian
ξ_f^d	=	desired elevation angle of the leader with respect to the follower in follower's vehicle-1 frame, radian
k_1, k_2	=	constant control gains
$\boldsymbol{p}_*$	=	inertial position of the $(*)$ leader or follower UAV, m.

*Ph.D. student, Department of Mechanical and Aerospace Engineering, Jett Hall Rm. 104, 1040 S. Horseshoe Street, Las Cruces, NM 88003.
†MSc student, Klipsch School of Electrical and Computer Engineering, Thomas & Brown Hall, 1125 Frenger Mall, Las Cruces, NM 88003.
‡Assistant Professor, Department of Mechanical and Aerospace Engineering, Jett Hall Rm. 104, 1040 S. Horseshoe Street, Las Cruces, NM 88003. AIAA Senior Member.

II. Introduction

Cooperative control (e..g, formation control, collision avoidance, etc.) for unmanned systems (e.g., self-driving automobiles, unmanned aerial vehicles (UAVs), and autonomous underwater vehicles (AUVs)) has gained more and more attention in research efforts due to its practical capability in diverse applications, such as self-driving car platoons [1–6], mobile agent formations [7], and platoons of autonomous underwater vehicles [8–11]. Besides these two-dimensional (2D) applications, formation control techniques for three-dimensional (3D) applications have also been explored [12–21]. However, almost all existing techniques for 3D formation control rely on global information sharing (e..g, the inertial coordinates of vehicles), which is subject to limited communication bandwidth, high power consumption of the Global Positioning System (GPS), together with high cost of accurate GPS devices, interference of GPS signals in congested environments (e.g., urban landscapes), and extra payload. These practical challenges call for 3D formation-control techniques that only use local information.

In the previous study for 3D global-information-based leader-follower formation control, Xuan-Mung and Kyung Hong [22] presented a robust adaptive formation controller based on a nonlinear model of the formation error dynamics. It considered both the relative position in the horizontal plane and the relative heading angle in the presence of uncertainties. Rafifandi et al. [23] reported the design and implementation of a leader-follower formation controller for two quadcopter UAVs with a ground station dictating a prescribed path for the leader. They developed a position tracking and a formation controllers with an accuracy of 50–115 cm. A centralized LQR-PI leader-follower formation controller for three quadcopters is proposed in [24], where the path of the leader is set as the two followers' desired paths.

Techniques based on the local-level frame or line-of-sight (LOS) frame have been reported in the literature [25–28]. In [26], a local-level spherical frame was used to develop a vision-based algorithm for a constant-speed UAV to avoid multiple stationary obstacles. The authors in [27, 28] developed formation controllers for a leader-follower UAV team to maintain a predefined 3D formation using local information only.

Previous studies for 3D formation control primarily assume absence of wind disturbances or a uniform wind field in the environment. To the best of our knowledge, no work has been reported that addresses all three challenges of 3D formation control: (1) converging to a 3D formation, (2) using only local information, and (3) considering generalized wind disturbances. This paper aims to fill this gap.

The contribution of this paper includes (1) a complete rigorous mathematical derivation of the relative dynamics of a leader-follower UAV team using a local-level spherical coordinate frame by taking wind disturbances into consideration, (2) a formation control law based on the backstepping technique, and (3) an estimator for wind-related terms in the derived relative dynamics. Simulations were conducted to verify the derived relative dynamics and the performance of the controller and estimator.

The remainder of this paper is structured as follows. The derivation of the relative dynamics is introduced in III. The wind estimation technique is presented in Section IV, followed by the observability analysis in Section V. The development of the formation controller and simulation results are presented in Sections VI and VII, respectively. Section VIII concludes the paper.

III. Derivation of the Relative Dynamics

A. Local-Level Frame

The local level frame is a body-centered relative coordinate system [29], where the x-axis points out of the nose of the unpitched vehicle frame, the y axis points out of the right wing of the un-rolled vehicle frame, and the z axis points down forming a right-handed coordinate system. The local level frame and associated symbols are defined and illustrated in Figs. 1, 2, and 3.

B. Derivation of Relative Dynamics

The line of sight LOS vector is given by

$$\boldsymbol{\rho}^i = \boldsymbol{p}_\ell - \boldsymbol{p}_f. \tag{1}$$

The velocities of the leader and follower UAVs are

$$\dot{\boldsymbol{p}}_\ell = \begin{pmatrix} V_{a\ell}\cos\gamma_{a\ell}\cos\psi_{a\ell} \\ V_{a\ell}\cos\gamma_{a\ell}\sin\psi_{a\ell} \\ -V_{a\ell}\sin\gamma_{a\ell} \end{pmatrix} + \begin{pmatrix} w_{\ell n} \\ w_{\ell e} \\ w_{\ell d} \end{pmatrix}, \tag{2}$$

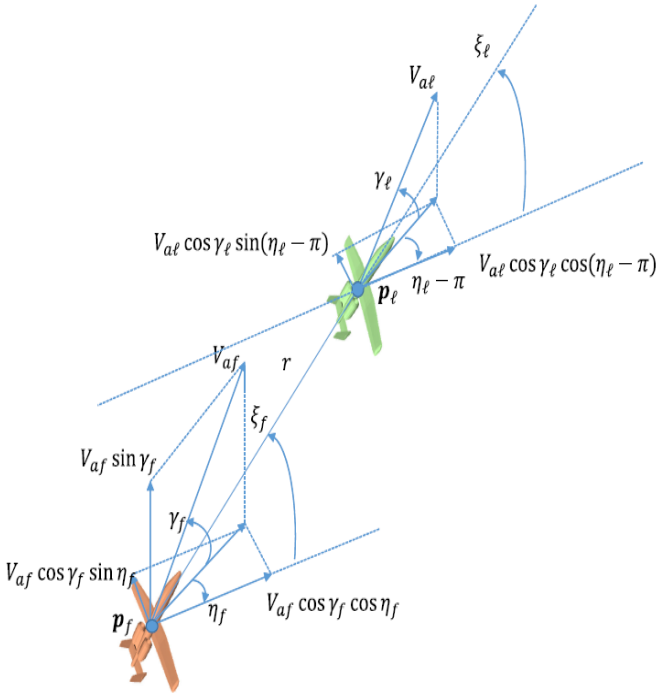

Fig. 1 Three-dimensional relative dynamics of a leader-follower unmanned aerial vehicle system based on a local level spherical coordinate frame.

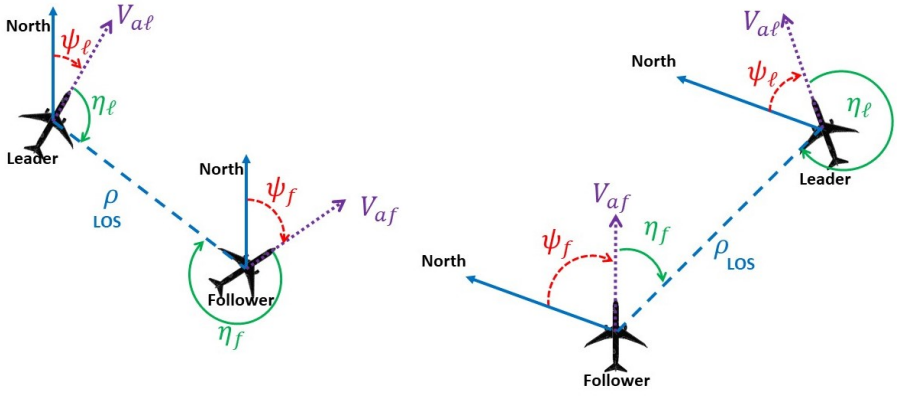

Fig. 2 2D relative lateral dynamics of a leader-follower unmanned aerial vehicle system.

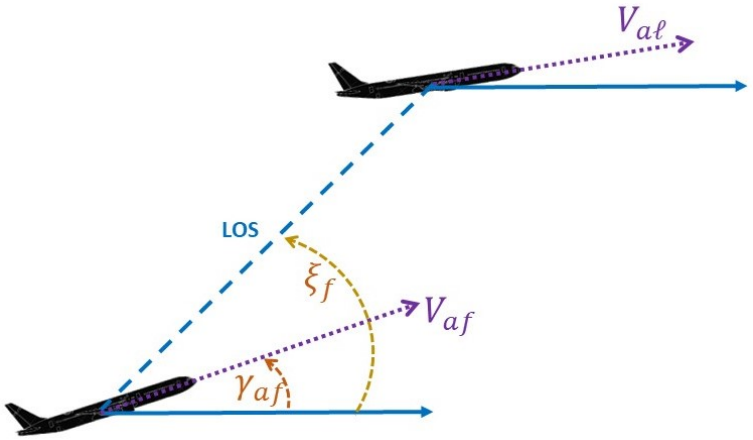

Fig. 3 2D relative longitudinal dynamics of a leader-follower unmanned aerial vehicle system.

$$\dot{\boldsymbol{p}}_f = \begin{pmatrix} V_{af}\cos\gamma_{af}\cos\psi_{af} \\ V_{af}\cos\gamma_{af}\sin\psi_{af} \\ -V_{af}\sin\gamma_{af} \end{pmatrix} + \begin{pmatrix} w_{fn} \\ w_{fe} \\ w_{fd} \end{pmatrix}. \tag{3}$$

The time derivative of the LOS vector, $\dot{\rho}$, is then given by

$$\dot{\boldsymbol{\rho}}^i = \dot{\boldsymbol{p}}_\ell - \dot{\boldsymbol{p}}_f \tag{4}$$

$$= \begin{pmatrix} V_{a\ell}\cos\gamma_{a\ell}\cos\psi_\ell - V_{af}\cos\gamma_{af}\cos\psi_f + (w_{\ell n} - w_{fn}) \\ V_{a\ell}\cos\gamma_{a\ell}\sin\psi_\ell - V_{af}\cos\gamma_{af}\sin\psi_f + (w_{\ell e} - w_{fe}) \\ -V_{a\ell}\sin\gamma_\ell + V_{af}\sin\gamma_{af} + (w_{\ell d} - w_{fd}) \end{pmatrix}. \tag{5}$$

The rotation matrix that rotates a vector from the inertial frame into the LOS frame, i.e., the rotation about the body-y and body-z axes, is given by

$$R_i^{\text{LOS}} = R_y R_z, \tag{6}$$

where

$$R_y = \begin{pmatrix} \cos\xi_f & 0 & -\sin\xi_f \\ 0 & 1 & 0 \\ \sin\xi_f & 0 & \cos\xi_f \end{pmatrix}, \tag{7}$$

and

$$R_z = \begin{pmatrix} \cos\left(\psi_f + \eta_f\right) & \sin\left(\psi_f + \eta_f\right) & 0 \\ -\sin\left(\psi_f + \eta_f\right) & \cos\left(\psi_f + \eta_f\right) & 0 \\ 0 & 0 & 1 \end{pmatrix}. \tag{8}$$

Then we have

$$R_i^{\text{LOS}} = \begin{pmatrix} \cos\xi_f\cos\left(\psi_f + \eta_f\right) & \cos\xi_f\sin\left(\psi_f + \eta_f\right) & -\sin\xi_f \\ -\sin\left(\psi_f + \eta_f\right) & \cos\left(\psi_f + \eta_f\right) & 0 \\ \sin\xi_f\cos\left(\psi_f + \eta_f\right) & \sin\xi_f\sin\left(\psi_f + \eta_f\right) & \cos\xi_f \end{pmatrix}. \tag{9}$$

The LOS rate, expressed in the LOS frame, is given by

$$\dot{\boldsymbol{\rho}}^{\text{LOS}} = R_i^{\text{LOS}}\dot{\boldsymbol{\rho}}^i. \tag{10}$$

Since we have

$$\Delta_{wn} = w_{\ell n} - w_{fn}, \tag{11}$$

$$\Delta_{we} = w_{\ell e} - w_{fe}, \tag{12}$$

$$\Delta_{wd} = w_{\ell d} - w_{fd}, \tag{13}$$

and $\xi_f = -\xi_\ell$, we can obtain

$$\begin{aligned}\dot{\boldsymbol{\rho}}^{\mathrm{LOS}}(1) = &-V_{a\ell}\left(\sin\gamma_{a\ell}\sin\xi_\ell + \cos\gamma_{a\ell}\cos\xi_\ell\cos\eta_\ell\right)\\ &- V_{af}\left(\sin\gamma_{af}\sin\xi_f + \cos\gamma_{af}\cos\xi_f\cos\eta_f\right)\\ &+ \cos\xi_f\left(\Delta_{wn}\cos\left(\psi_f+\eta_f\right) + \Delta_{we}\sin\left(\psi_f+\eta_f\right)\right) - \Delta_{wd}\sin\xi_f,\end{aligned} \tag{14}$$

$$\begin{aligned}\dot{\boldsymbol{\rho}}^{\mathrm{LOS}}(2) = &\, V_{a\ell}\cos\gamma_{a\ell}\sin\eta_\ell\\ &+ V_{af}\cos\gamma_{af}\sin\eta_f\\ &- \Delta_{wn}\sin\left(\psi_f+\eta_f\right) + \Delta_{we}\cos\left(\psi_f+\eta_f\right),\end{aligned} \tag{15}$$

$$\begin{aligned}\dot{\boldsymbol{\rho}}^{\mathrm{LOS}}(3) = &\, V_{a\ell}\left(\cos\gamma_{a\ell}\sin\xi_\ell\cos\eta_\ell - \sin\gamma_{a\ell}\cos\xi_\ell\right)\\ &+ V_{af}\left(\sin\gamma_{af}\cos\xi_f - \cos\gamma_{af}\sin\xi_f\cos\eta_f\right)\\ &+ \Delta_{wn}\sin\xi_f\cos\left(\psi_f+\eta_f\right) + \Delta_{we}\sin\xi_f\sin\left(\psi_f+\eta_f\right) + \Delta_{wd}\cos\xi_f.\end{aligned} \tag{16}$$

In the LOS frame, the radial and tangential components in the lateral and longitudinal directions are defined as

$$\dot{\boldsymbol{\rho}}^{\mathrm{LOS}} \triangleq \begin{bmatrix}\dot{\rho}_{\mathrm{r}}\\ \dot{\rho}_{lat}\\ \dot{\rho}_{lon}\end{bmatrix}. \tag{17}$$

From the dynamics shown in Fig. 1, the change in the LOS vector in the radial direction $\dot{\rho}_{\mathrm{r}}$, lateral tangential direction $\dot{\rho}_{lat}$, and the longitudinal tangential direction $\dot{\rho}_{lon}$ can be expressed as

$$\begin{bmatrix}\dot{\rho}_{\mathrm{r}}\\ \dot{\rho}_{lat}\\ \dot{\rho}_{lon}\end{bmatrix} = \begin{bmatrix}\dot{r}\\ r\cos\xi_f\left(\dot{\psi}_f+\dot{\eta}_f\right)\\ -r\left(\dot{\xi}_f\right)\end{bmatrix}. \tag{18}$$

Using the aforementioned relationships and expressions, we can obtain

$$\begin{aligned}\dot{r} = &-V_{a\ell}\left(\sin\gamma_{a\ell}\sin\xi_\ell + \cos\gamma_{a\ell}\cos\xi_\ell\cos\eta_\ell\right)\\ &- V_{af}\left(\sin\gamma_{af}\sin\xi_f + \cos\gamma_{af}\cos\xi_f\cos\eta_f\right)\\ &+ \cos\xi_f\left(\Delta_{wn}\cos\left(\psi_f+\eta_f\right) + \Delta_{we}\sin\left(\psi_f+\eta_f\right)\right) - \Delta_{wd}\sin\xi_f,\end{aligned} \tag{19}$$

$$\begin{aligned}\dot{\eta}_f = &\frac{1}{r\cos\xi_f}\left(V_{a\ell}\cos\gamma_{a\ell}\sin\eta_\ell + V_{af}\cos\gamma_{af}\sin\eta_f\right)\\ &+ \frac{1}{r\cos\xi_f}\left(-\Delta_{wn}\sin\left(\psi_f+\eta_f\right) + \Delta_{we}\cos\left(\psi_f+\eta_f\right)\right) - \dot{\psi}_f,\end{aligned} \tag{20}$$

$$\begin{aligned}\dot{\eta}_\ell = &\frac{1}{r\cos\xi_\ell}\left(V_{a\ell}\cos\gamma_{a\ell}\sin\eta_\ell + V_{af}\cos\gamma_{af}\sin\eta_f\right)\\ &+ \frac{1}{r\cos\xi_\ell}\left(-\Delta_{wn}\sin\left(\psi_f+\eta_f\right) + \Delta_{we}\cos\left(\psi_f+\eta_f\right)\right) - \dot{\psi}_\ell,\end{aligned} \tag{21}$$

$$\dot{\xi}_f = -\frac{V_{a\ell}}{r}\left(\cos\gamma_{a\ell}\sin\xi_\ell\cos\eta_\ell - \sin\gamma_{a\ell}\cos\xi_\ell\right) \tag{22}$$
$$-\frac{V_{af}}{r}\left(\sin\gamma_{af}\cos\xi_f - \cos\gamma_{af}\sin\xi_f\cos\eta_f\right)$$
$$-\frac{1}{r}\left(\Delta_{wn}\sin\xi_f\cos\left(\psi_f+\eta_f\right) + \Delta_{we}\sin\xi_f\sin\left(\psi_f+\eta_f\right) + \Delta_{wd}\cos\xi_f\right).$$

Letting $\rho = \frac{1}{r}$, then $\dot{r} = -\frac{1}{\rho^2}\dot{\rho}$, we have

$$\dot{\rho} = \rho^2 V_{a\ell}\left(\sin\gamma_{a\ell}\sin\xi_\ell + \cos\gamma_{a\ell}\cos\xi_\ell\cos\eta_\ell\right) \tag{23}$$
$$+\rho^2 V_{af}\left(\sin\gamma_{af}\sin\xi_f + \cos\gamma_{af}\cos\xi_f\cos\eta_f\right)$$
$$-\rho^2\cos\xi_f\left(\Delta_{wn}\cos\left(\psi_f+\eta_f\right) + \Delta_{we}\sin\left(\psi_f+\eta_f\right)\right) + \rho^2\Delta_{wd}\sin\xi_f,$$

$$\dot{\eta}_f = \frac{\rho}{\cos\xi_f}\left(V_{a\ell}\cos\gamma_{a\ell}\sin\eta_\ell + V_{af}\cos\gamma_{af}\sin\eta_f\right) \tag{24}$$
$$+\frac{\rho}{\cos\xi_f}\left(-\Delta_{wn}\sin\left(\psi_f+\eta_f\right) + \Delta_{we}\cos\left(\psi_f+\eta_f\right)\right) - \dot{\psi}_f,$$

$$\dot{\eta}_\ell = \frac{\rho}{\cos\xi_\ell}\left(V_{a\ell}\cos\gamma_{a\ell}\sin\eta_\ell + V_{af}\cos\gamma_{af}\sin\eta_f\right) \tag{25}$$
$$+\frac{\rho}{\cos\xi_\ell}\left(-\Delta_{wn}\sin\left(\psi_\ell+\eta_\ell\right) + \Delta_{we}\cos\left(\psi_\ell+\eta_\ell\right)\right) - \dot{\psi}_\ell,$$

$$\dot{\xi}_f = -\rho V_{a\ell}\left(\cos\gamma_{a\ell}\sin\xi_\ell\cos\eta_\ell - \sin\gamma_{a\ell}\cos\xi_\ell\right) \tag{26}$$
$$-\rho V_{af}\left(\sin\gamma_{af}\cos\xi_f - \cos\gamma_{af}\sin\xi_f\cos\eta_f\right)$$
$$-\rho\left(\Delta_{wn}\sin\xi_f\cos\left(\psi_f+\eta_f\right) + \Delta_{we}\sin\xi_f\sin\left(\psi_f+\eta_f\right) + \Delta_{wd}\cos\xi_f\right).$$

IV. Wind Estimation

To estimate the wind terms in Eqns. (23) to (26), we develop an extended Kalman filter (EKF) in this section, followed by the observability analysis in Section V.

A. Extended Kalman Filter (EKF)

The EKF for wind speed estimation is summarized in Algorithm 1. In a nutshell, the EKF is an iterative process using sequential noisy measurements (y), a priori knowledge of the state ($\hat{x}$), system inputs (u), and the physical models (f and h) to update a state estimation and its covariance matrix (P). The EKF keeps predicting the state until the measured sensor data are available. Then, the EKF compares the predicted output ($h(\hat{x}, u)$) to the actual sensor data (y) and corrects the state estimation accordingly.

The system dynamics model (f) represents how the states evolve over time given the inputs u and the system state in the previous time step. In the prediction step, the system dynamics model is directly used to produce a prediction of the states (line 5). The covariance matrix is predicted by using the Jacobian matrix (A), which is calculated by performing the partial derivative of the system dynamics with respect to the state vector (line 6). Matrix A is then used to update the covariance matrix (P) of the estimation error (line 7) [30], associated with the covariance matrix (Q) of the system process noise, which is generally unknown and therefore becomes a system gain that can be tuned to improve the performance of the EKF [30].

In the measurement step, matrix C is calculated by taking the partial derivative of the system output function (h) with respect to the state vector (line 10). Matrix C is used to compute the optimal Kalman Gain L_i (line 11), used to decide how much of the new measurement (y_i) will contribute to the update of the covariance (line 12) and the state estimation (line 13). A large Kalman Gain implies that sensor measurements are more accurate.

Algorithm 1 Continuous-Discrete Extended Kalman Filter [30]

Initialize: $\hat{x} = 0$.
Pick an output sample rate T_{out}, which is much less than the sample rates of the sensors.
At each sample time T_{out} :
for i = 1 to N {Prediction Step} **do**
    $\hat{x} = \hat{x} + \left(\frac{T_{out}}{N}\right) f(\hat{x}, u)$
    $A = \frac{\partial f}{\partial x}(\hat{x}, u)$
    $P = P + \left(\frac{T_{out}}{N}\right)\left(AP + PA^T + Q\right)$
end for
if Measurement has been received from sensor i {Measurement Update} **then**
    $C_i = \frac{\partial h_i}{\partial x}(\hat{x}, u[n])$
    $L_i = PC_i^T\left(R_i + C_i P C_i^T\right)^{-1}$
    $P = (I - L_i C_i) P$
    $\hat{x} = \hat{x} + L_i\left(y_i[n] - h(\hat{x}, u[n])\right)$
end if

B. Wind Estimation Using EKF

In this section, the superscript "e" is used to denote all variables related to estimation. The state vector, $x^e \in \mathbb{R}^7$, is defined as

$$x^e \triangleq \left(\rho, \eta_\ell, \eta_f, \xi_f, \Delta_{\omega_n}, \Delta_{\omega_e}, \Delta_{\omega_d}\right)^T, \tag{27}$$

and the system dynamics is given by

$$\dot{x}^e = f(x^e) \triangleq \begin{bmatrix} \dot{\rho} & \dot{\eta}_\ell & \dot{\eta}_f & \dot{\xi}_f & 0 & 0 & 0 \end{bmatrix}^T. \tag{28}$$

The output vector is defined by

$$y^e \triangleq h(x^e) = \left(x_1^e, x_2^e, x_3^e, x_4^e\right)^T. \tag{29}$$

Then, matrix C is given by

$$C = \frac{\partial h}{\partial x^e} = \begin{bmatrix} 1 & 0 & 0 & 0 & 0 & 0 & 0 \\ 0 & 1 & 0 & 0 & 0 & 0 & 0 \\ 0 & 0 & 1 & 0 & 0 & 0 & 0 \\ 0 & 0 & 0 & 1 & 0 & 0 & 0 \end{bmatrix}, \tag{30}$$

and matrix A is calculated by

$$A = \frac{\partial f}{\partial x^e} = [A_{ij}] = \begin{bmatrix} A_{11} & A_{12} & A_{13} & A_{14} & A_{15} & A_{16} & A_{17} \\ A_{21} & A_{22} & A_{23} & 0 & A_{25} & A_{26} & 0 \\ A_{31} & A_{32} & A_{33} & A_{34} & A_{35} & A_{36} & 0 \\ A_{41} & A_{42} & A_{43} & A_{44} & A_{45} & A_{46} & A_{47} \\ 0 & 0 & 0 & 0 & 0 & 0 & 0 \\ 0 & 0 & 0 & 0 & 0 & 0 & 0 \\ 0 & 0 & 0 & 0 & 0 & 0 & 0 \end{bmatrix}, \tag{31}$$

where

$$\begin{aligned} A_{11} &= \frac{\partial f_1}{\partial x_1^e} = 2x_1^e x_7 \sin\left(x_4^e\right) - 2x_1 \cos\left(x_4^e\right)\left(x_5 \cos\left(\psi_f + x_3^e\right) + x_6 \sin\left(\psi_f + x_3^e\right)\right) \\ &+ 2V_{af} x_1^e \left(\sin\left(\gamma_{af}\right) \sin\left(x_4^e\right) + \cos\left(\gamma_{af}\right) \cos\left(x_3^e\right) \cos\left(x_4^e\right)\right) \\ &+ 2V_{al} x_1^e \left(\sin\left(\gamma_{a\ell}\right) \sin\left(\xi_\ell\right) + \cos\left(\gamma_{a\ell}\right)\left(\gamma_{a\ell}\right) \cos\left(x_2^e\right) \cos\left(\xi_\ell\right)\right), \end{aligned}$$

$$A_{12} = \frac{\partial f_1}{\partial x_2^e} = -V_{al} x_1^{e2} \cos\left(\gamma_{a\ell}\right) \cos\left(\xi_\ell\right) \sin\left(x_2^e\right),$$

$$A_{13} = \frac{\partial f_1}{\partial x_3^e} = -x_1^{e2}\cos\left(x_4^e\right)\left(x_6^e\cos\left(\psi_f + x_3^e\right) - x_5\sin\left(\psi_f + x_3^e\right)\right)$$
$$- V_{af}x_1^{e2}\cos\left(\gamma_{af}\right)\cos\left(x_4^e\right)\sin\left(x_3^e\right),$$

$$A_{14} = \frac{\partial f_1}{\partial x_4^e} = x_1^{e2}x_7^e\cos\left(x_4^e\right) + x_1^{e2}\sin\left(x_4^e\right)\left(x_5^e\cos\left(\psi_f + x_3^e\right) + x_6^e\sin\left(\psi_f + x_3^e\right)\right)$$
$$+ V_{af}x_1^{e2}\left(\sin\left(\gamma_{af}\right)\cos\left(x_4^e\right) - \cos\left(\gamma_{af}\right)\cos\left(x_3^e\right)\sin\left(x_4^e\right)\right),$$

$$A_{15} = \frac{\partial f_1}{\partial x_5^e} = -x_1^{e2}\cos\left(\psi_f + x_3^e\right)\cos\left(x_4^e\right),$$

$$A_{16} = \frac{\partial f_1}{\partial x_6^e} = -x_1^{e2}\sin\left(\psi_f + x_3^e\right)\cos\left(x_4^e\right),$$

$$A_{17} = \frac{\partial f_1}{\partial x_7^e} = x_1^{e2}\sin\left(x_4^e\right),$$

$$A_{21} = \frac{\partial f_2}{\partial x_1^e} = \frac{1}{cos(\xi_\ell)}\left(x_6^e\cos\left(\psi_\ell + x_2^e\right) - x_5^e\sin\left(\psi_\ell + x_2^e\right)\right)$$
$$+ \frac{1}{cos(\xi_\ell)}\left(V_{af}\cos\left(\gamma_{af}\right)\sin\left(x_3^e\right) + V_{al}\cos\left(\gamma_{a\ell}\right)\sin\left(x_2^e\right)\right),$$

$$A_{22} = \frac{\partial f_2}{\partial x_2^e} = \frac{1}{cos(\xi_\ell)}\left(V_{al}x_1^e\cos\left(\gamma_{a\ell}\right)\cos\left(x_2^e\right)\right) - \frac{1}{cos(\xi_\ell)}\left(x_1^e\left(x_5^e\cos\left(\psi_\ell + x_2^e\right) + x_6^e\sin\left(\psi_\ell + x_2^e\right)\right)\right),$$

$$A_{23} = \frac{\partial f_2}{\partial x_3^e} = \frac{V_{af}x_1^e\cos\left(\gamma_{af}\right)\cos\left(x_3^e\right)}{\cos\left(\xi_\ell\right)},$$

$$A_{25} = \frac{\partial f_2}{\partial x_5^e} = -\frac{x_1\sin\left(\psi_\ell + x_2^e\right)}{\cos\left(\xi_\ell\right)},$$

$$A_{26} = \frac{\partial f_2}{\partial x_6^e} = \frac{x_1^e\cos\left(\psi_\ell + x_2^e\right)}{\cos\left(\xi_\ell\right)},$$

$$A_{31} = \frac{\partial f_3}{\partial x_1^e} = \frac{1}{\cos x_4^e}\left(x_6^e\cos\left(\psi_f + x_3^e\right) - x_5^e\sin\left(\psi_f + x_3^e\right)\right)$$
$$+ \frac{1}{\cos x_4^e}\left(V_{af}\cos\left(\gamma_{af}\right)\sin(x_3^e) + V_{al}\cos\left(\gamma_{a\ell}\right)\sin\left(x_2^e\right)\right),$$

$$A_{32} = \frac{\partial f_3}{\partial x_2^e} = \frac{V_{al}x_1^e\cos\left(\gamma_{a\ell}\right)\cos\left(x_2^e\right)}{\cos x_4^e},$$

$$A_{33} = \frac{\partial f_3}{\partial x_3^e} = \frac{V_{af}x_1^e\cos\left(\gamma_{af}\right)\cos\left(x_3^e\right)}{\cos x_4^e}$$
$$- \frac{1}{\cos x_4}\left(x_1^e\left(x_5^e\cos\left(\psi_f + x_3^e\right) + x_6^e\sin\left(\psi_f + x_3^e\right)\right)\right),$$

$$A_{34} = \frac{\partial f_3}{\partial x_4^e} = \frac{1}{\cos^2 x_4^e}\left(x_1^e\sin\left(x_4^e\right)\left(V_{af}\cos\left(\gamma_{af}\right)\sin\left(x_3^e\right) + V_{al}\cos\left(\gamma_{a\ell}\right)\sin\left(x_2^e\right)\right)\right)$$
$$+ \frac{1}{\cos^2 x_4^e}\left(x_1^e\sin\left(x_4^e\right)\left(x_6^e\cos\left(\psi_f + x_3^e\right) - x_5^e\sin\left(\psi_f + x_3^e\right)\right)\right),$$

$$A_{35} = \frac{\partial f_3}{\partial x_5^e} = -\frac{x_1^E\sin\left(\psi_f + x_3^e\right)}{\cos x_4^e},$$

$$A_{36} = \frac{\partial f_3}{\partial x_6^e} = \frac{x_1^e\cos\left(\psi_f + x_3^e\right)}{\cos x_4^e},$$

$$A_{41} = \frac{\partial f_4}{\partial x_1^e} = V_{al}\left(\sin\left(\gamma_{a\ell}\right)\cos\left(\xi_\ell\right) - \cos\left(\gamma_{a\ell}\right)\cos\left(x_2^e\right)\sin\left(\xi_\ell\right)\right)$$
$$- x_5^e\cos\left(\psi_f + x_3^e\right)\sin\left(x_4^e\right) - x_6^e\sin\left(\psi_f + x_3^e\right)\sin\left(x_4^e\right)$$
$$- V_{af}\left(\sin\left(\gamma_{af}\right)\cos(x_4^e) - \cos\left(\gamma_{af}\right)\cos\left(x_3^e\right)\sin\left(x_4^e\right)\right) - x_7^e\cos\left(x_4^e\right),$$

$$A_{42} = \frac{\partial f_4}{\partial x_2^e} = V_{al}x_1^e\cos\left(\gamma_{a\ell}\right)\sin\left(x_2^e\right)\sin\left(\xi_\ell\right),$$

$$A_{43} = \frac{\partial \dot{x}_4^e}{\partial x_3^e} = -x_1^e \left(x_6^e \cos\left(\psi_f + x_3^e\right) \sin\left(x_4^e\right) - x_5^e \sin\left(\psi_f + x_3^e\right) \sin\left(x_4^e\right)\right)$$
$$- V_{af} x_1^e \cos\left(\gamma_{af}\right) \sin\left(x_3^e\right) \sin\left(x_4^e\right),$$

$$A_{44} = \frac{\partial f_4}{\partial x_4^e} = V_{af} x_1^e \left(\sin\left(\gamma_{af}\right) \sin\left(x_4^e\right) + \cos\left(\gamma_{af}\right) \cos\left(x_3^e\right) \cos\left(x_4^e\right)\right)$$
$$- x_1^e \left(x_5^e \cos\left(\psi_f + x_3^e\right) \cos\left(x_4^e\right) - x_7^e \sin\left(x_4^e\right) + x_6^e \sin\left(\psi_f + x_3^e\right) \cos\left(x_4^e\right)\right),$$

$$A_{45} = \frac{\partial f_4}{\partial x_5^e} = -x_1^e \cos\left(\psi_f + x_3^e\right) \sin\left(x_4^e\right),$$

$$A_{46} = \frac{\partial f_4}{\partial x_6^e} = -x_1^e \sin\left(\psi_f + x_3^e\right) \sin\left(x_4^e\right),$$

$$A_{47} = \frac{\partial f_4}{x_7^e} = -x_1^e \cos\left(x_4^e\right).$$

V. Observability Analysis

The observability of a system refers to whether a system state can be found using specified system outputs in a finite time. In other words, the "ability to perform state estimation depends on whether sufficient measurements are well distributed throughout the system" [31, 32]. So the external outputs can be used to find the hidden states of the entire system if the system is observable. The observability matrix of the nonlinear system, described by Equations (28) and (29) is defined by

$$O \triangleq \begin{bmatrix} \frac{\partial \mathcal{L}_f^0 h}{\partial x} & \frac{\partial \mathcal{L}_f^1 h}{\partial x} & \frac{\partial \mathcal{L}_f^2 h}{\partial x} & \frac{\partial \mathcal{L}_f^3 h}{\partial x} & \frac{\partial \mathcal{L}_f^4 h}{\partial x} & \frac{\partial \mathcal{L}_f^5 h}{\partial x} & \frac{\partial \mathcal{L}_f^6 h}{\partial x} \end{bmatrix}^T, \tag{32}$$

where $\mathcal{L}_f^0 h = h$ and $\mathcal{L}_f^n h = \frac{\partial \mathcal{L}_f^{n-1} h}{\partial x} f$. Then, we have

$$\mathcal{L}_f^1 h = \frac{\partial \mathcal{L}_f^0 h}{\partial x} f = \frac{\partial h}{\partial x} f, \tag{33}$$

where

$$\frac{\partial h}{\partial x} = \begin{bmatrix} 1 & 0 & 0 & 0 & 0 & 0 & 0 \\ 0 & 1 & 0 & 0 & 0 & 0 & 0 \\ 0 & 0 & 1 & 0 & 0 & 0 & 0 \\ 0 & 0 & 0 & 1 & 0 & 0 & 0 \end{bmatrix}. \tag{34}$$

We can also obtain

$$\mathcal{L}_f^2 h = \frac{\partial \mathcal{L}_f^1 h}{\partial x} f, \tag{35}$$

where

$$\frac{\partial \mathcal{L}_f^1 h}{\partial x} = \begin{bmatrix} \frac{\partial_f^1 \mathbf{f}_1^e}{\partial x_1^e} & \frac{\partial_f^1 \mathbf{f}_1^e}{\partial x_2^e} & \frac{\partial_f^1 \mathbf{f}_1^e}{\partial x_3^e} & \frac{\partial_f^1 \mathbf{f}_1^e}{\partial x_4^e} & -x_1^{e2} \cos\left(\psi_f + x_3\right) \cos\left(x_4^e\right) & x_1^{e2} \sin\left(\psi_f + x_3\right) \cos\left(x_4^e\right) & x_1^{e2} \sin(x_4^e) \\ \frac{\partial_f^1 \mathbf{f}_2^e}{\partial x_1^e} & \frac{\partial_f^1 \mathbf{f}_2^e}{\partial x_2^e} & \frac{\partial_f^1 \mathbf{f}_2^e}{\partial x_3^e} & \frac{\partial_f^1 \mathbf{f}_2^e}{\partial x_4^e} & -\frac{x_1^e \sin\left(\psi_f + x_3\right)}{\cos\left(x_4^e\right)} & \frac{x_1^e \cos\left(\psi_f + x_3\right)}{\cos\left(x_4^e\right)} & 0 \\ \frac{\partial_f^1 \mathbf{f}_3^e}{\partial x_1^e} & \frac{\partial_f^1 \mathbf{f}_3^e}{\partial x_2^e} & \frac{\partial_f^1 \mathbf{f}_3^e}{\partial x_3^e} & \frac{\partial_f^1 \mathbf{f}_3^e}{\partial x_4^e} & -\frac{x_1^e \sin\left(\psi_\ell + x_2\right)}{\cos(\xi_\ell)} & \frac{x_1^e \cos\left(\psi_\ell + x_2\right)}{\cos(\xi_\ell)} & 0 \\ \frac{\partial_f^1 \mathbf{f}_4^e}{\partial x_1^e} & \frac{\partial_f^1 \mathbf{f}_4^e}{\partial x_2^e} & \frac{\partial_f^1 \mathbf{f}_4^e}{\partial x_3^e} & \frac{\partial_f^1 \mathbf{f}_4^e}{\partial x_4^e} & -x_1^e \cos\left(\psi_f + x_3\right) \sin\left(x_4^e\right) & -x_1^e \sin\left(\psi_f + x_3\right) \sin\left(x_4^e\right) & -x_1^e \cos\left(x_4^e\right) \end{bmatrix} \tag{36}$$

The first eight rows of matrix O form a new matrix, O', which is given by

$$O' \triangleq \begin{bmatrix} 1 & 0 & 0 & 0 & 0 & 0 & 0 \\ 0 & 1 & 0 & 0 & 0 & 0 & 0 \\ 0 & 0 & 1 & 0 & 0 & 0 & 0 \\ 0 & 0 & 0 & 1 & 0 & 0 & 0 \\ \frac{\partial^1_f \mathbf{f}^e_1}{\partial x^e_1} & \frac{\partial^1_f \mathbf{f}^e_1}{\partial x^e_2} & \frac{\partial^1_f \mathbf{f}^e_1}{\partial x^e_3} & \frac{\partial^1_f \mathbf{f}^e_1}{\partial x^e_4} & -x_1^{e2}\cos\left(\psi_f + x_3\right)\cos\left(x_4^e\right) & x_1^{e2}\sin\left(\psi_f + x_3\right)\cos\left(x_4^e\right) & x_1^{e2}\sin(x_4^e) \\ \frac{\partial^1_f \mathbf{f}^e_2}{\partial x^e_1} & \frac{\partial^1_f \mathbf{f}^e_2}{\partial x^e_2} & \frac{\partial^1_f \mathbf{f}^e_2}{\partial x^e_3} & \frac{\partial^1_f \mathbf{f}^e_2}{\partial x^e_4} & -\frac{x_1^e \sin(\psi_f + x_3)}{\cos\left(x_4^e\right)} & \frac{x_1^e \cos(\psi_f + x_3)}{\cos\left(x_4^e\right)} & 0 \\ \frac{\partial^1_f \mathbf{f}^e_3}{\partial x^e_1} & \frac{\partial^1_f \mathbf{f}^e_3}{\partial x^e_2} & \frac{\partial^1_f \mathbf{f}^e_3}{\partial x^e_3} & \frac{\partial^1_f \mathbf{f}^e_3}{\partial x^e_4} & -\frac{x_1^e \sin(\psi_\ell + x_2)}{\cos(\xi_\ell)} & \frac{x_1^e \cos(\psi_\ell + x_2)}{\cos(\xi_\ell)} & 0 \\ \frac{\partial^1_f \mathbf{f}^e_4}{\partial x^e_1} & \frac{\partial^1_f \mathbf{f}^e_4}{\partial x^e_2} & \frac{\partial^1_f \mathbf{f}^e_4}{\partial x^e_3} & \frac{\partial^1_f \mathbf{f}^e_4}{\partial x^e_4} & -x_1^e\cos\left(\psi_f + x_3\right)\sin\left(x_4^e\right) & -x_1^e\sin\left(\psi_f + x_3\right)\sin\left(x_4^e\right) & -x_1^e\cos\left(x_4^e\right) \end{bmatrix} \tag{37}$$

Excluding row 7 from matrix O', we can obtain a new squared matrix

$$\Omega \triangleq \begin{bmatrix} 1 & 0 & 0 & 0 & 0 & 0 & 0 \\ 0 & 1 & 0 & 0 & 0 & 0 & 0 \\ 0 & 0 & 1 & 0 & 0 & 0 & 0 \\ 0 & 0 & 0 & 1 & 0 & 0 & 0 \\ \frac{\partial^1_f \mathbf{f}^e_1}{\partial x^e_1} & \frac{\partial^1_f \mathbf{f}^e_1}{\partial x^e_2} & \frac{\partial^1_f \mathbf{f}^e_1}{\partial x^e_3} & \frac{\partial^1_f \mathbf{f}^e_1}{\partial x^e_4} & -x_1^{e2}\cos\left(\psi_f + x_3\right)\cos\left(x_4^e\right) & x_1^{e2}\sin\left(\psi_f + x_3\right)\cos\left(x_4^e\right) & x_1^{e2}\sin(x_4^e) \\ \frac{\partial^1_f \mathbf{f}^e_2}{\partial x^e_1} & \frac{\partial^1_f \mathbf{f}^e_2}{\partial x^e_2} & \frac{\partial^1_f \mathbf{f}^e_2}{\partial x^e_3} & \frac{\partial^1_f \mathbf{f}^e_2}{\partial x^e_4} & -\frac{x_1^e \sin(\psi_f + x_3)}{\cos\left(x_4^e\right)} & \frac{x_1^e \cos(\psi_f + x_3)}{\cos\left(x_4^e\right)} & 0 \\ \frac{\partial^1_f \mathbf{f}^e_4}{\partial x^e_1} & \frac{\partial^1_f \mathbf{f}^e_4}{\partial x^e_2} & \frac{\partial^1_f \mathbf{f}^e_4}{\partial x^e_3} & \frac{\partial^1_f \mathbf{f}^e_4}{\partial x^e_4} & -x_1^e\cos\left(\psi_f + x_3\right)\sin\left(x_4^e\right) & -x_1^e\sin\left(\psi_f + x_3\right)\sin\left(x_4^e\right) & -x_1^e\cos\left(x_4^e\right) \end{bmatrix}. \tag{38}$$

The determinant of Ω is

$$|\Omega| = \frac{\left(x_1^e\right)^4}{\cos\left(x_4^e\right)}. \tag{39}$$

Then, the system is observable, if $|\Omega| \neq 0$, which implies that $x_1^e \neq 0$ and $x_4^e \neq \frac{\pi}{2}$, i.e., $\rho \neq 0$ and $\xi_f \neq \frac{\pi}{2}$. Since ρ is the inverse of the distance between the leader and follower UAVs, which is always nonzero, the system is observable if the leader is not right above the follower.

VI. Formation Control Law

In this section, we consider a desired formation defined by r^d (or ρ^d), η_f^d , and ξ_f^d that can be achieved by controlling V_{af}, η_f, and γ_{af}.

A. Controller Design

In this paper, the desired formation vector $\alpha^d = \left(\rho^d, \eta_\ell^d, \xi_f^d\right)$ is assumed constant, i.e., $\dot{\alpha} = \mathbf{0}$. Defining

$$\alpha = \begin{pmatrix} \rho \\ \eta_\ell \\ \xi_f \end{pmatrix} \tag{40}$$

we have

$$\dot{\alpha} = f(\alpha) + g \cdot u, \tag{41}$$

$$u \triangleq \begin{pmatrix} \dot{V}_{af} \\ \dot{\eta}_f \\ \dot{\gamma}_{af} \end{pmatrix}. \tag{42}$$

Then, the tracking error dynamics can be obtained

$$e_\alpha = \alpha - \alpha^d \tag{43}$$

$$\dot{e}_\alpha = \dot{\alpha} - \dot{\alpha}^d \tag{44}$$

$$= f(\alpha) + g - \dot{\alpha}^d \tag{45}$$

Define a candidate Lyapunov function as

$$V_1 \triangleq \frac{1}{2} \|e_\alpha\|^2, \tag{46}$$

and tts time derivative is

$$\dot{V}_1 = e_\alpha^T \dot{e}_\alpha \tag{47}$$

$$= e_\alpha^T (f(\alpha) + g - \dot{\alpha}^d). \tag{48}$$

At this stage we consider f as a virtual control input to make $\dot{V}_1$ negative. We introduce a new error variable

$$z \triangleq -g + \dot{\alpha}^d - k_1 e_\alpha - f, \tag{49}$$

We have

$$f = \dot{\alpha}^d - k_1 e_\alpha - g - z \tag{50}$$

and

$$\dot{e}_\alpha = f + g - \dot{\alpha}^d \tag{51}$$

$$= -k_1 e_\alpha - z. \tag{52}$$

Then we have

$$\dot{V}_1 = e_\alpha^T \dot{e}_\alpha \tag{53}$$

$$= e_\alpha^T (-k_1 e_\alpha - z) \tag{54}$$

$$= -e_\alpha^T z - k_1 \|e_\alpha\|^2 \tag{55}$$

Consider an augmented Lyapunov function

$$V_2 = V_1 + \frac{1}{2} \|z\|^2 \tag{56}$$

which has the time derivative as

$$\dot{V}_2 = \dot{V}_1 + z^T \dot{z} \tag{57}$$

Since

$$\dot{z} = -\frac{dg}{dt} + \ddot{\alpha}^d - k_1 \dot{e}_\alpha \tag{58}$$

we have

$$\dot{V}_2 = e_\alpha^T z - k_1 \|e_\alpha\|^2 + z^T (\ddot{\alpha}^d - \frac{dg}{dt} - k_1 \dot{e}_\alpha) \tag{59}$$

$$= -k_1 \|e_\alpha\|^2 + e_\alpha^T z + z^T (\ddot{\alpha}^d - \frac{dg}{dt} - k_1 \dot{e}_\alpha) \tag{60}$$

Let

$$\frac{dg}{dt} = \frac{\partial g}{\partial \alpha}\dot{\alpha} + \frac{\partial g}{\partial u}\dot{u}. \tag{61}$$

where

$$\frac{\partial g}{\partial \alpha} \triangleq A = \begin{pmatrix} A_{11} & A_{12} & A_{13} \\ A_{21} & A_{22} & A_{23} \\ A_{31} & A_{32} & A_{33} \end{pmatrix}, \tag{62}$$

$$\frac{\partial g}{\partial u} \triangleq B = \begin{pmatrix} B_{11} & B_{12} & B_{13} \\ B_{21} & B_{22} & B_{23} \\ B_{31} & B_{32} & B_{33} \end{pmatrix}, \tag{63}$$

with

$$\begin{aligned} A_{11} = \frac{\partial \dot{\rho}}{\partial \rho} &= 2\rho V_{a\ell}\left(\sin\gamma_{a\ell}\sin\xi_\ell + \cos\gamma_{a\ell}\cos\xi_\ell\cos\eta_\ell\right) \\ &+ 2\rho V_{af}\left(\sin\gamma_{af}\sin\xi_f + \cos\gamma_{af}\cos\xi_f\cos\eta_f\right) \\ &-2\rho\cos\xi_f\left(\Delta_{wn}\cos\left(\psi_f+\eta_f\right) + \Delta_{we}\sin\left(\psi_f+\eta_f\right)\right) + 2\rho\Delta_{wd}\sin\xi_f, \end{aligned} \tag{64}$$

$$A_{12} = \frac{\partial \dot{\rho}}{\partial \eta_\ell} = -\rho^2 V_{a\ell}\left(\cos\gamma_{a\ell}\cos\xi_\ell\sin\eta_\ell\right), \tag{65}$$

$$\begin{aligned} A_{13} = \frac{\partial \dot{\rho}}{\partial \xi_f} &= \rho^2 V_{a\ell}\left(-\sin\gamma_{a\ell}\cos\xi_f - \cos\gamma_{a\ell}\sin\xi_f\cos\eta_\ell\right) \\ &+ \rho^2 V_{af}\left(\sin\gamma_{af}\cos\xi_f - \cos\gamma_{af}\sin\xi_f\cos\eta_f\right) \\ &+\rho^2\sin\xi_f\left(\Delta_{wn}\cos\left(\psi_f+\eta_f\right) + \Delta_{we}\sin\left(\psi_f+\eta_f\right)\right) + \rho^2\Delta_{wd}\cos\xi_f, \end{aligned} \tag{66}$$

$$\begin{aligned} A_{21} = \frac{\partial \dot{\eta}_f}{\partial \rho} &= \frac{1}{\cos\xi_f}\left(V_{a\ell}\cos\gamma_{a\ell}\sin\eta_\ell + V_{af}\cos\gamma_{af}\sin\eta_f\right) \\ &+ \frac{1}{\cos\xi_f}\left(-\Delta_{wn}\sin\left(\psi_f+\eta_f\right) + \Delta_{we}\cos\left(\psi_f+\eta_f\right)\right), \end{aligned} \tag{67}$$

$$A_{22} = \frac{\partial \dot{\eta}_f}{\partial \eta_\ell} = \frac{\rho}{\cos\xi_f}\left(V_{a\ell}\cos\gamma_{a\ell}\cos\eta_\ell\right), \tag{68}$$

$$\begin{aligned} A_{23} = \frac{\partial \dot{\eta}_f}{\partial \xi_f} &= \frac{\rho\sin\xi_f}{\cos^2\xi_f}\left(V_{a\ell}\cos\gamma_{a\ell}\sin\eta_\ell + V_{af}\cos\gamma_{af}\sin\eta_f\right) \\ &+ \frac{\rho\sin\xi_f}{\cos^2\xi_f}\left(-\Delta_{wn}\sin\left(\psi_f+\eta_f\right) + \Delta_{we}\cos\left(\psi_f+\eta_f\right)\right), \end{aligned} \tag{69}$$

$$\begin{aligned} A_{31} = \frac{\partial \dot{\xi}_f}{\partial \rho} &= -V_{a\ell}\left(\cos\gamma_{a\ell}\sin\xi_\ell\cos\eta_\ell - \sin\gamma_{a\ell}\cos\xi_\ell\right) \\ &- V_{af}\left(\sin\gamma_{af}\cos\xi_f - \cos\gamma_{af}\sin\xi_f\cos\eta_f\right) \\ &- \left(\Delta_{wn}\sin\xi_f\cos\left(\psi_f+\eta_f\right) + \Delta_{we}\sin\xi_f\sin\left(\psi_f+\eta_f\right) + \Delta_{wd}\cos\xi_f\right), \end{aligned} \tag{70}$$

$$A_{32} = \frac{\partial \dot{\xi}_f}{\partial \eta_\ell} = \rho V_{a\ell} \left(\cos\gamma_{a\ell} \sin\xi_\ell \sin\eta_\ell\right), \tag{71}$$

$$\begin{aligned} A_{33} = \frac{\partial \dot{\xi}_f}{\partial \xi_f} &= \rho V_{a\ell} \left(\cos\gamma_{a\ell} \cos\xi_f \cos\eta_\ell - \sin\gamma_{a\ell} \sin\xi_f\right) \\ &+ \rho V_{af} \left(\sin\gamma_{af} \sin\xi_f + \cos\gamma_{af} \cos\xi_f \cos\eta_f\right) \\ &- \rho \left(\Delta_{wn} \cos\xi_f \cos\left(\psi_f + \eta_f\right) + \Delta_{we} \cos\xi_f \sin\left(\psi_f + \eta_f\right) - \Delta_{wd} \sin\xi_f\right), \end{aligned} \tag{72}$$

$$B_{11} = \frac{\partial \dot{\rho}}{\partial V_{af}} = \rho^2 \big(\sin\gamma_{af} \sin\xi_f + \cos\gamma_{af} \cos\xi_f \cos\eta_f\big), \tag{73}$$

$$\begin{aligned} B_{12} = \frac{\partial \dot{\rho}}{\partial \eta_f} &= -\rho^2 V_{af} \left(\cos\gamma_{af} \cos\xi_f \sin\eta_f\right) \\ &-\rho^2 \cos\xi_f \left(-\Delta_{wn} \sin\left(\psi_f + \eta_f\right) + \Delta_{we} \cos\left(\psi_f + \eta_f\right)\right), \end{aligned} \tag{74}$$

$$B_{13} = \frac{\partial \dot{\rho}}{\partial \gamma_{af}} = \rho^2 V_{af} \left(\cos\gamma_{af} \sin\xi_f - \sin\gamma_{af} \cos\xi_f \cos\eta_f\right), \tag{75}$$

$$B_{21} = \frac{\partial \dot{\eta}_f}{\partial V_{af}} = \frac{\rho}{\cos\xi_f} \left(\cos\gamma_{af} \sin\eta_f\right), \tag{76}$$

$$\begin{aligned} B_{22} = \frac{\partial \dot{\eta}_f}{\partial \eta_f} &= \frac{\rho}{\cos\xi_f} \left(V_{af} \cos\gamma_{af} \cos\eta_f\right) \\ &+ \frac{\rho}{\cos\xi_f} \left(-\Delta_{wn} \cos\left(\psi_f + \eta_f\right) - \Delta_{we} \sin\left(\psi_f + \eta_f\right)\right), \end{aligned} \tag{77}$$

$$B_{23} = \frac{\partial \dot{\eta}_f}{\partial \gamma_{af}} = \frac{\rho}{\cos\xi_f} \left(-V_{af} \sin\gamma_{af} \sin\eta_f\right), \tag{78}$$

$$B_{31} = \frac{\partial \dot{\xi}_f}{\partial V_{af}} = -\rho \left(\sin\gamma_{af} \cos\xi_f - \cos\gamma_{af} \sin\xi_f \cos\eta_f\right), \tag{79}$$

$$\begin{aligned} B_{32} = \frac{\partial \dot{\xi}_f}{\partial \eta_f} &= -\rho V_{af} \left(\cos\gamma_{af} \sin\xi_f \sin\eta_f\right) \\ &- \rho \sin\xi_f \left(-\Delta_{wn} \sin\left(\psi_f + \eta_f\right) + \Delta_{we} \cos\left(\psi_f + \eta_f\right)\right), \end{aligned} \tag{80}$$

$$B_{33} = \frac{\partial \dot{\xi}_f}{\partial \gamma_{af}} = -\rho V_{af} \left(\cos\gamma_{af} \cos\xi_f + \sin\gamma_{af} \sin\xi_f \cos\eta_f\right). \tag{81}$$

Matrix $B(I_f(t))$ is invertible if $\left|B(I_f(t))\right| = -\frac{\rho^4 V_{af}^2 \cos\gamma_{af}}{\cos\xi_f} \neq 0$, which implies that $\rho \neq 0$, $V_{af} \neq 0$, and $\xi_f \neq \frac{\pi}{2}$. Since ρ is the inverse of the distance between the leader and follower UAVs, which is always nonzero, and $V_{af} \neq 0$ is always true for a fixed-wing UAV, the system is observable if the leader is not right above the follower.

$$\dot{u} = B^{-1} \left[k_2 z - k_1 \dot{e}_\alpha - e_\alpha + \ddot{\alpha}^d - A\dot{\alpha}\right]. \tag{82}$$

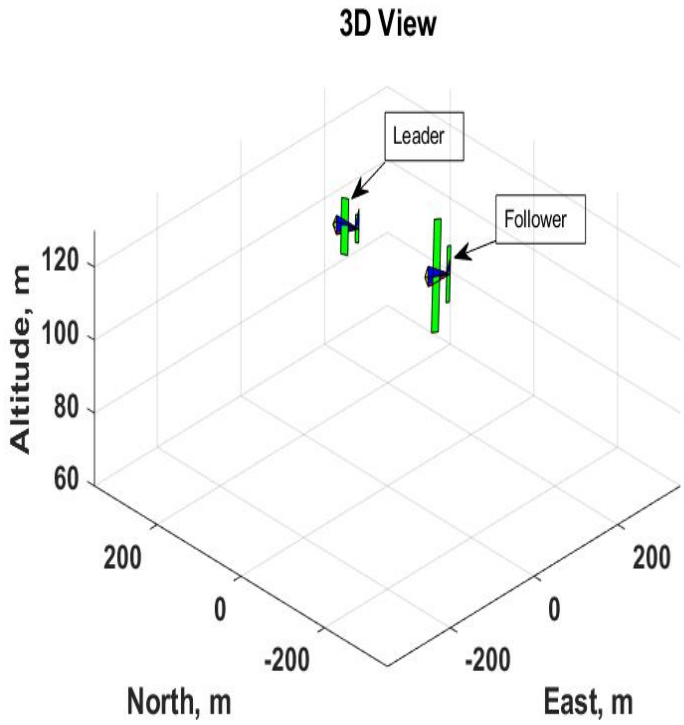

Fig. 4 Screen shot of a simulation run.

VII. Simulations Results

In order to evaluate the performance and feasibility achieved by the derived relative dynamics and the formation controller described in Sections III and VI, numerical simulations were performed using MATLAB/ Simulink (see Fig. 4). The follower UAV keeps a predefined formation with respect to the leader UAV using the local information of the two UAVs, i.e., the relative distance, elevation angles and azimuth angles. The leader UAV transmits its relative azimuth angle, flight path angle, and airspeed to the follower UAV. As shown in Figs. 5 and 6 The leader was commanded to follow a circular path (red line) with a constant airspeed of 25 m/s while the follower (blue line) converges to the formation with a relative desired distance of 50 m (see top subfigure in Fig. 8). In Fig. 8, it also shows that the leader azimuth angle η_l converged to the desired value of -100 degrees. The bottom subfigure in Fig. 8 shows ξ_f follows a desired angle of 20 degrees. Figure 7 confirms that the error in the distance and the fore-mentioned angles are converging to zero. The controller commands are shown in Fig. 9.

VIII. Conclusion

In this paper, the relative dynamics were developed for a leader-follower UAV team, under the presence of wind. A backstepping based formation control law was then developed using only the leader-follower's local information. Based on the derived dynamics model, the observability analysis was conducted and an extended Kalman filter was developed to estimate the wind difference between the leader and follower UAVs. The proposed controller was tested under different wind conditions and the simulation results show the effectiveness of the controller under an example wind condition for a leader-follower UAV system to maintain a desired 3D formation where the leader was following a circular orbit.

Acknowledgments

This research was supported by the NASA New Mexico Space Grant Consortium (NMSGC) under the Research Infrastructure Development program.

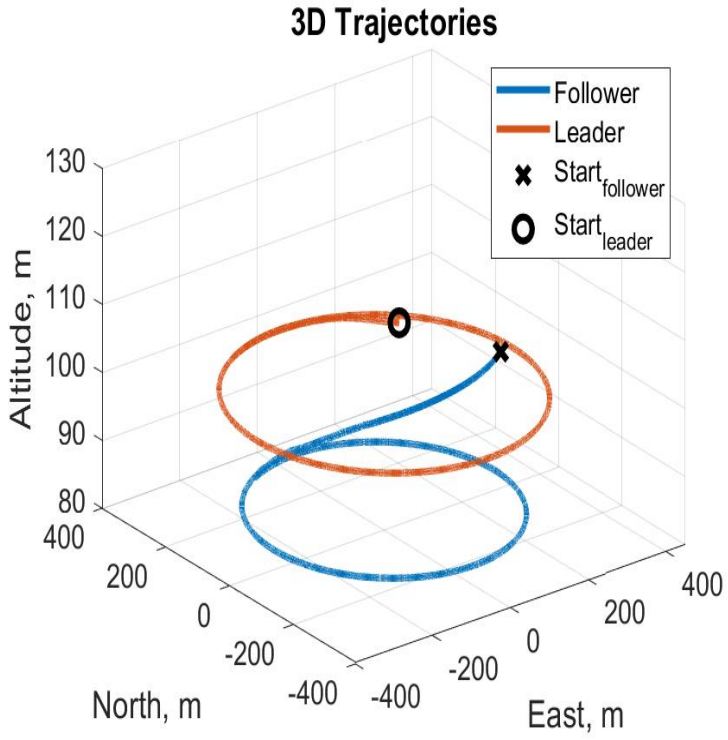

Fig. 5 3D View of the leader and follower trajectories.

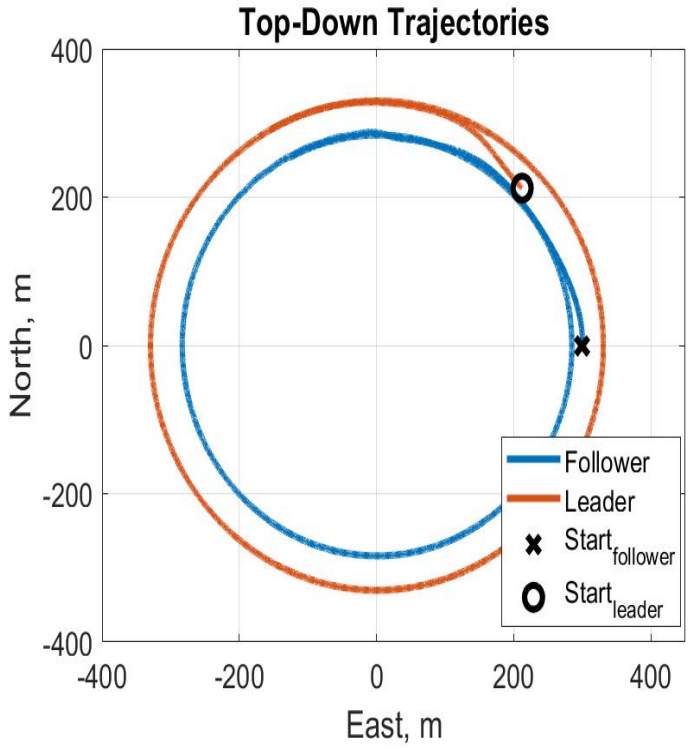

Fig. 6 Top-Down view of the trajectories of the leader and follower.

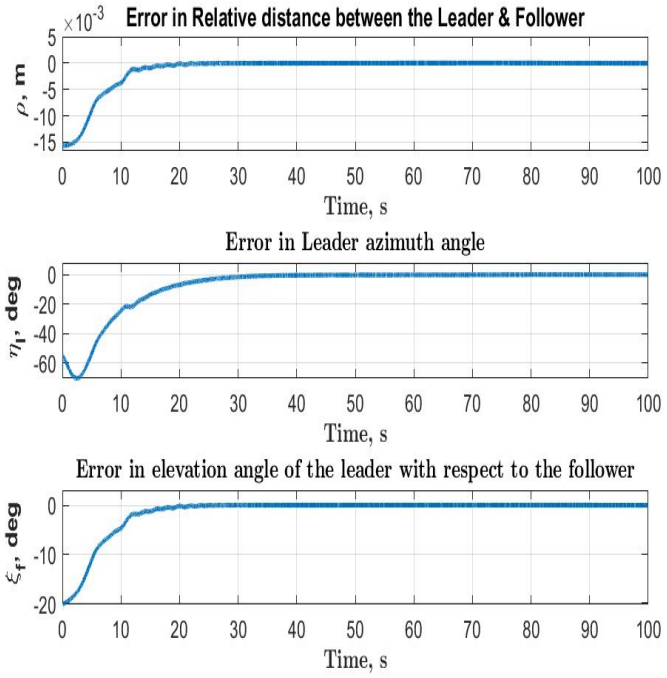

Fig. 7 Distance and angles error.

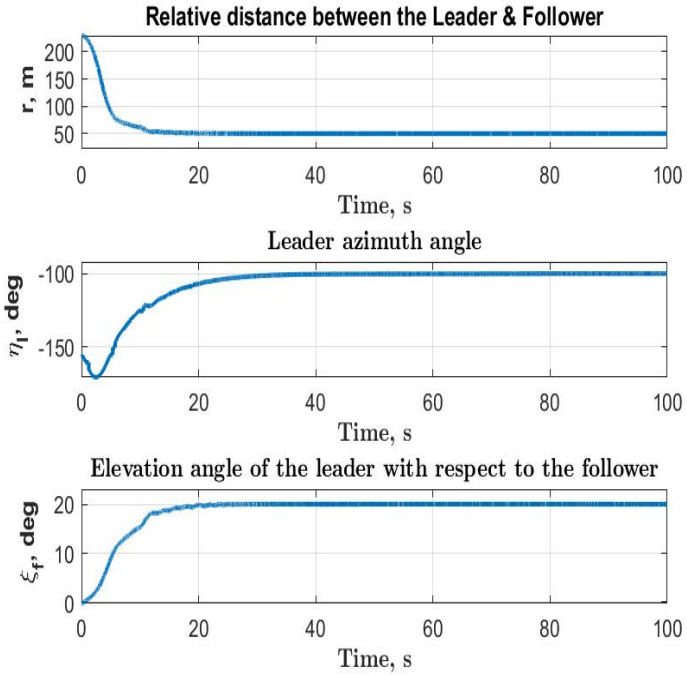

Fig. 8 States: Distance and angles of the leader and follower UAVs.

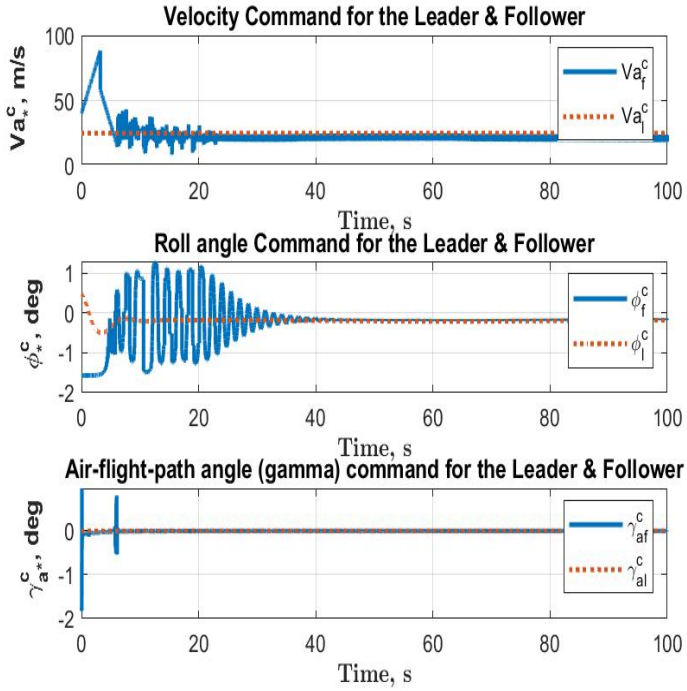

Fig. 9 Controller commands to the leader and Follower UAVs.

References

[1] Ploeg, J., Van De Wouw, N., and Nijmeijer, H., "Lp string stability of cascaded systems: Application to vehicle platooning," *IEEE Transactions on Control Systems Technology*, Vol. 22, No. 2, 2013, pp. 786–793.

[2] Hu, B., and Lemmon, M. D., "Distributed switching control to achieve almost sure safety for leader-follower vehicular networked systems," *IEEE Transactions on Automatic Control*, Vol. 60, No. 12, 2015, pp. 3195–3209.

[3] Alam, A., Gattami, A., Johansson, K. H., and Tomlin, C. J., "Guaranteeing safety for heavy duty vehicle platooning: Safe set computations and experimental evaluations," *Control Engineering Practice*, Vol. 24, 2014, pp. 33–41.

[4] Lygeros, J., Godbole, D. N., and Sastry, S., "Verified hybrid controllers for automated vehicles," *IEEE transactions on automatic control*, Vol. 43, No. 4, 1998, pp. 522–539.

[5] Swaroop, D., and Hedrick, J. K., "String stability of interconnected systems," *IEEE transactions on automatic control*, Vol. 41, No. 3, 1996, pp. 349–357.

[6] Stilwell, D. J., and Bishop, B., "A strategy for controlling autonomous robot platoons," *Proceedings of the 39th IEEE Conference on Decision and Control (Cat. No. 00CH37187)*, Vol. 4, IEEE, 2000, pp. 3483–3488.

[7] Tanner, H. G., Pappas, G. J., and Kumar, V., "Leader-to-formation stability," *IEEE Trans. Robot. Autom.*, Vol. 20, No. 3, 2004, pp. 443–455. doi:10.1109/TRA.2004.825275.

[8] Stilwell, D. J., and Bishop, B. E., "Platoons of underwater vehicles," *IEEE Control Systems Magazine*, Vol. 20, No. 6, 2000, pp. 45–52.

[9] Stilwell, D. J., and Bishop, B. D., "Communication, Feedback and Decentralized Control for Platoons of Underwater Vehicles," Tech. rep., Naval Academy Annapolis MD div of Engineering and Weapons, 2000.

[10] Cui, R., Ge, S. S., How, B. V. E., and Choo, Y. S., "Leader–follower formation control of underactuated autonomous underwater vehicles," *Ocean Engineering*, Vol. 37, No. 17-18, 2010, pp. 1491–1502.

[11] Shojaei, K., "Leader-follower formation control of underactuated autonomous marine surface vehicles with limited torque," *Ocean Engineering*, Vol. 105, 2015, pp. 196–205.

[12] Kim, S., and Kim, Y., "Three dimensional optimum controller for multiple UAV formation flight using behavior-based decentralized approach," *2007 International Conference on Control, Automation and Systems*, IEEE, 2007, pp. 1387–1392.

[13] Kim, S., Kim, Y., and Tsourdos, A., "Optimized behavioural UAV formation flight controller design," *2009 European Control Conference (ECC)*, IEEE, 2009, pp. 4973–4978.

[14] Choi, J., and Kim, Y., "Fuel efficient three dimensional controller for leader-follower UAV formation flight," *2007 International Conference on Control, Automation and Systems*, IEEE, 2007, pp. 806–811.

[15] Shan, J., and Liu, H.-T., "Close-formation flight control with motion synchronization," *Journal of Guidance, Control, and Dynamics*, Vol. 28, No. 6, 2005, pp. 1316–1320.

[16] Kim, S., and Kim, Y., "Optimum design of three-dimensional behavioural decentralized controller for UAV formation flight," *Engineering Optimization*, Vol. 41, No. 3, 2009, pp. 199–224.

[17] Liu, H., Wang, X., and Zhu, H., "A novel backstepping method for the three-dimensional multi-UAVs formation control," *2015 IEEE International Conference on Mechatronics and Automation (ICMA)*, IEEE, 2015, pp. 923–928.

[18] Yang, Q., Cao, M., Fang, H., and Chen, J., "Constructing Universally Rigid Tensegrity Frameworks With Application in Multiagent Formation Control," *IEEE Transactions on Automatic Control*, Vol. 64, No. 1, 2019, pp. 378–385.

[19] Paul, T., Krogstad, T. R., and Gravdahl, J. T., "UAV formation flight using 3D potential field," *2008 16th Mediterranean Conference on Control and Automation*, IEEE, 2008, pp. 1240–1245.

[20] Sun, L., Huo, W., and Jiao, Z., "Adaptive backstepping control of spacecraft rendezvous and proximity operations with input saturation and full-state constraint," *IEEE Transactions on Industrial Electronics*, Vol. 64, No. 1, 2016, pp. 480–492.

[21] Jin, C., Zhu, M., Sun, L., and Zheng, Z., "Relative motion modeling and control for a quadrotor landing on an unmanned vessel," *AIAA Guidance, Navigation, and Control Conference*, 2017, p. 1522.

[22] Xuan-Mung, N., and Hong, S. K., "Robust adaptive formation control of quadcopters based on a leader–follower approach," *International Journal of Advanced Robotic Systems*, Vol. 16, No. 4, 2019, p. 1729881419862733.

[23] Rafifandi, R., Asri, D. L., Ekawati, E., and Budi, E. M., "Leader–follower formation control of two quadrotor UAVs," *SN Applied Sciences*, Vol. 1, No. 6, 2019, p. 539.

[24] Ali, Q., and Montenegro, S., "Explicit model following distributed control scheme for formation flying of mini UAVs," *IEEE Access*, Vol. 4, 2016, pp. 397–406.

[25] Nichols, J. W., Sun, L., Beard, R. W., and McLain, T., "Aerial Rendezvous of Small Unmanned Aircraft Using a Passive Towed Cable System," *J. Guid. Control. Dyn.*, Vol. 37, No. 4, 2014, pp. 1131–1142. doi:10.2514/1.62220, URL `http://arc.aiaa.org/doi/10.2514/1.62220`.

[26] Yu, H., and Beard, R. W., "Vision-based local-level frame mapping and planning in spherical coordinates for miniature air vehicles," *IEEE Trans. Control Syst. Technol.*, Vol. 21, No. 3, 2013, pp. 695–703. doi:10.1109/TCST.2012.2190604.

[27] Sun, L., Hu, B., and Zhao, S., "An Event-Triggering-Based Approach for Three-Dimensional Local-Level Frame Formation Control of Leader-Follower UAVs," 2017.

[28] Sun, L., and Hu, B., "Event-triggering in three-dimensional leader-follower formation control for unmanned aerial vehicles," *ASME 2016 Dyn. Syst. Control Conf.*, 2016.

[29] Sahawneh, Laith R and Beard, R. W., "Path Planning in the Local-Level Frame for Small Unmanned Aircraft Systems," *Intech open*, Vol. 2, 2017, p. 64. doi:10.5772/32009.

[30] Beard, R. W., and McLain, T. W., *Small unmanned aircraft: Theory and practice*, Princeton university press, 2012.

[31] Monticelli, A., *State Estimation in Electric Power Systems*, Springer Science+Business Media New York, Boston, MA, 1999, pp. 161–199.

[32] Al-Radaidehl, A., and Sun, L., "Observability Analysis and Bayesian Filtering for Self-Localization of a Tethered Multicopter in GPS-Denied Environments," *2019 International Conference on Unmanned Aircraft Systems (ICUAS)*, IEEE, 2019, pp. 1041–1047.